

## Monte Carlo Simulation of Submicron Devices and Processes

Lyliane Rajaonarison, Patrice Hesto, Jean-François Pône, Philippe Dollfus

*Institut d'Electronique Fondamentale, CNRS URA022, Université Paris-Sud, 91405 ORSAY Cedex,  
France*

### Abstract

In this paper, we present the MONACO program which includes a particle simulation of three-dimensional processes (actually limited to localized implantations) and a two-dimensional simulation of the electrical behaviour of submicron devices. These two models use Monte-Carlo methods and they can treat submicron components with any geometry. For instance, some results about a MOSFET with a gate dimension of  $0.1 \times 0.5 \mu\text{m}^2$  will be shown.

## 1 Introduction

Today the improvements of electron beam lithography allow the fabrication of ultra-submicron Field Effect Transistors with high performances. For example, MOSFET with  $0.1 \mu\text{m}$  gate length and  $0.5 \mu\text{m}$  gate width have been fabricated by IBM<sup>(1)</sup>. These MOSFET exhibit a maximum transconductance  $g_m$  greater than 600 mS/mm at 300K and 900 mS/mm at 77K. But two problems occur for studying and predicting the performances of these devices : in the channel, electron transport is non-stationary and the number of impurity atoms under the gate is very low. For example, the doping level in the channel of the IBM MOSFET is about  $N_A \approx 4 \times 10^{17} \text{cm}^{-3}$  which corresponds to 1,500 impurity atoms in the space charge layer for the inversion mode. Many computer programs include both the processes and the electrical simulations : FEDESS and FIELDAY from IBM, SUPREM and PISCES from Stanford, TITAN and JUPIN from CNET, IMPACT from ISEN, but they generally deal with the processes in a macroscopic way and the electron transport is simulated by the drift-diffusion method. They are not well suited for the study of ultra-submicron components. For these reasons, we develop the MONACO program which allows the simulation of processes as well as the electrical operation taking into account

the geometry issued from the processes. Today, the processes which can be treated by MONACO are limited to localized implantations.

## 2 Simulation of the localized implantation

### 2.1 The model

The algorithm is induced from the Monte-Carlo method. It consists of following the trajectory of every ion until it comes to rest. Every incident ion moves in straight free-flight-paths, separated by binary collisions with the target atoms. The ion direction is assumed to change as a result of these collisions. Its energy is transferred part to the electronic cloud around its trajectory and part to the "knock-on" atoms. The interaction between incident ion and target ion is treated by a classical mechanical approach with a randomly selected impact parameter. The interaction potential is the Moliere's potential at low energies and the Coulomb's potential at high energies. For the electronic energy losses, we take a calculation according to the LSS (Lindhard-Scharff-Schiott) theory at low energies and the Bethe and Bloch's equations at high energies<sup>(2)</sup>.

Actually, our program does not take into account the channeling phenomena which result from ion scattering into the crystallographic directions of the material. On the other hand, it can deal with all geometries and all chemical compounds. It has been extended in order to include multilayer structures. The transition (laterally or in depth) between two materials is immediately detected because the free-flight-paths are kept equal to the mean atomic spacing in the target. The nuclear and electronic stopping powers are assumed to be independent and are changed according to the chemical composition of the material. The "knock-on" atom is randomly chosen with respect to the material stoichiometry. Then, our program can simulate the ion implantation in a whole process of any electronic device realization.

### 2-2 Results for the 0.1 $\mu$ m MOSFET

We have simulated the implantation steps of the fabrication of a 0.1x0.5 $\mu$ m<sup>2</sup> MOSFET with the true number of implanted impurity atoms and the various masks used in a self-aligned technology. A schematic cross section of the device is drawn in Fig.1.

The ion implantations are made on a 0.5x0.5 $\mu$ m<sup>2</sup> area with an incidence angle normal to the target. The main processing steps are summarized below :

a)-For the channel :

Boron is implanted into the substrate with 6,400 ions at 15keV ( $\cong 3.2 \times 10^{12} \text{cm}^{-2}$ ) and 15,400 ions at 30keV ( $\cong 7.7 \times 10^{12} \text{cm}^{-2}$ ). The distribution of boron ions is shown in Fig.2a. We can notice fluctuations for this distribution with few impurities under the gate oxide, as well as the overdoping in depth introduced in order to limit the punch-through phenomena resulting from the short channel effects.

b)-For the source and drain extensions :

Antimony implantations into the source and drain extensions is realized through the 4.5nm thick gate oxide on which is deposited the  $100 \times 100 \text{nm}^2$  polysilicon gate, and are grown the overall 7.5nm thick SiO<sub>2</sub> layer : 25,000 ions at 10keV ( $\cong 1.25 \times 10^{13} \text{cm}^{-2}$ ) and 79,500 ions at 20keV ( $\cong 4 \times 10^{13} \text{cm}^{-2}$ ). These extensions are necessary to delimit the channel length. Indeed, in order to ensure a shallow junction near the channel and small lateral stragglings under the gate, low energy implantations are useful. Figure 2b shows the antimony distribution. We can see a small overflow of the S-D extension zones which reduces the effective gate length. Several donor impurities are stopped by the polysilicon, but some ions reach the channel via the S-D zones and could disturb the electrical device operation.

c)-For the source and drain contact areas :

Arsenic is implanted into the source and drain contact zones using a sidewall 100nm thick Si<sub>3</sub>N<sub>4</sub> gate spacer with 770,000 ions at 20keV ( $\cong 3.9 \times 10^{14} \text{cm}^{-2}$ ). The relative high dose allows to obtain low access S-D resistances, but lateral diffusion is made larger (see fig.2-c). Hence, in order to offset the N<sup>+</sup> implant, a sidewall spacer is introduced. A large part of ions are stopped into Si<sub>3</sub>N<sub>4</sub>. Some donor impurities meet the channel side via the S-D regions, but they are in the extension zones, and have there no influence on the electrical behaviour of the device.

### 3 Simulation of the electrical behaviour

#### 3.1 The model

The electrical simulation includes both the description of the electron motion using a particle Monte-Carlo model taking into account the electric field, and the resolution of Poisson's equation, considering the applied bias voltages and the distribution of the electric charges. This simulator has been described previously<sup>(3)</sup>. It can describe the dynamic of electrons and holes in a device with any shape, 15 electrodes and 30 various materials at most. Carrier-phonon scattering involve both acoustic and optical phonons, with coupling by deformation potential and by Coulomb interaction for polar materials. For simple cases, a 2DK approach exists. For the conduction band, we have a three valley model  $\Gamma$  L X (if they exist) and for the valence band, a two valley model (heavy and light holes). We take into account the energy band non-parabolicity. The ohmic contact zones are modelled by

Generation-Recombination centers with infinite velocity. The effect of an ionizing particle (generation of electron-hole pairs along the track) can also be treated. We use a classical approach for the heterojunction crossing. For the resolution of the Poisson's equation, the carrier densities are means over space and over time. The time step is inferior to the smallest dielectric relaxation time (in the highest doped zone) and the mesh size is rectangular (cell lengths are about the Debye's length).

### 3-2 Results for the 0.1 $\mu\text{m}$ MOSFET

Concerning the electrical behaviour of the 0.1x0.5 $\mu\text{m}^2$  MOSFET, we have only simulated the dotted rectangular plotted in Fig.1. We have taken a large part of drain extension in order that electrons can thermalize themselves before reaching the drain contact. The number of impurity atoms per mesh used to calculate the potential is derived from the implantation simulations. We notice, considering the small dimensions of the device, that it works with the true number of impurity atoms and carriers (30,000 in this case). On the other hand, we take thin meshing (mesh dimensions, in the channel, under the gate, are 2x2.5nm<sup>2</sup>); this means that the distribution of acceptor atoms is very noisy because inside each mesh there are 0, 1 or 2 atoms (see Fig.3). The same phenomena occur in the source and drain regions. Nevertheless, our computer program is still stable.

Figure 6 displays the  $I_{\text{DS}}-V_{\text{DS}}$  characteristics for fixed  $V_{\text{GS}}$  with error bars on current amplitude. There is a good saturation of  $I_{\text{DS}}$ . This figure also shows the variations of the saturation current  $I_{\text{DSsat}}$  versus  $V_{\text{GS}}$ . It is worth noting that this current increases linearly with the gate voltage, this means that the saturation phenomena do not come from the channel pinch off (in this case  $I_{\text{DSsat}}$  would be proportional to the square of  $V_{\text{GS}}-V_{\text{T}}$ ). Furthermore the transconductance  $g_{\text{m}}$  is about 800 mS/mm.

We have investigated the electron behaviour in the channel. At every time, we know the position, the kinetic energy and the velocity components of each electron. Figure 5 shows the distribution of the mean velocity in the source-drain direction for the electrons, in a 20nm thick channel parallel to the oxide interface under the gate. We note that this velocity increases throughout the channel and reaches 3.5x10<sup>7</sup>cm.s<sup>-1</sup> at the drain side, against the interface. As the saturation velocity of electrons in silicon is less than 10<sup>7</sup>cm.s<sup>-1</sup>, we can conclude that electron transport is non-stationary. This means that electrons suffer only few scattering during their motion in the channel. In silicon, two main types of interaction occur with about the same frequencies: elastic scattering (acoustic, impurity) and inelastic scattering with emission of a 50 meV phonon (non-polar optic and equivalent intervalley interactions). In these conditions, the variations of the total energy (kinetic energy + potential energy) of the electrons give the number of inelastic interactions suffered by electrons during their transit across the channel. The total carrier energy is plotted in Fig.6. The dotted line represents the maximum energy of electrons in the channel, if they were purely ballistic. In fact, they lose an energy of about 0.3eV which

corresponds to the emission of about 6 phonons. This value falls in good agreement with the frequency of inelastic interactions ( $\approx 10^{13}$  Hz) which yields one interaction every 0.1ps , that is about 7 phonon emissions during the transit time ( $\approx 0.7$ ps).

#### **4 Conclusion**

We have developed a particle ensemble Monte-Carlo model allowing the simulation of both the processes (actually limited to localized implantations) and the electrical behaviour of submicron devices. The programs take into account the problems coming from the decrease of the component dimensions (the spatial distribution of impurity atoms and the non-stationary transport phenomena).

#### **References**

- (1) KERN,D.P., 19th European Solid State Device Research Conference, Berlin, 1989, (Eds., Heuberger,A., Ryssel,H., Lange,P., Springer-Verlag), p.633
- (2) BIRSACK,J.P., HAGGMARK,L.G., Nucl. Instr. and Meth., 174, (1980), p257
- (3) HESTO,P., PONE,J-F, MOUIS,M., PELOUARD,J-L., CASTAGNE,R., Nasescode IV Conference, Dublin, 1985, (Ed., Miller,J.J.H., Boole Press), p315

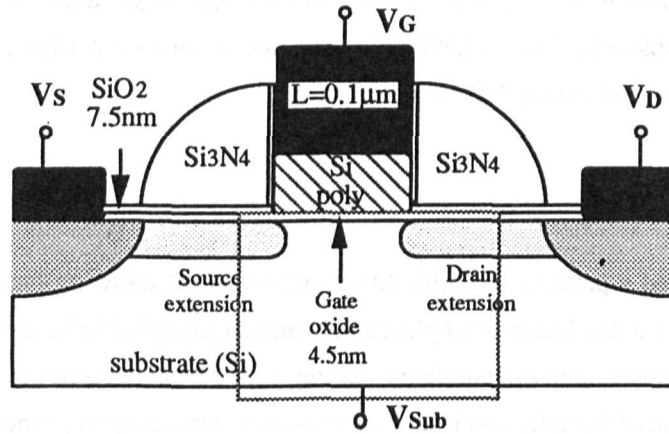


Figure 1: Cross section of the 100nm gate length MOSFET.

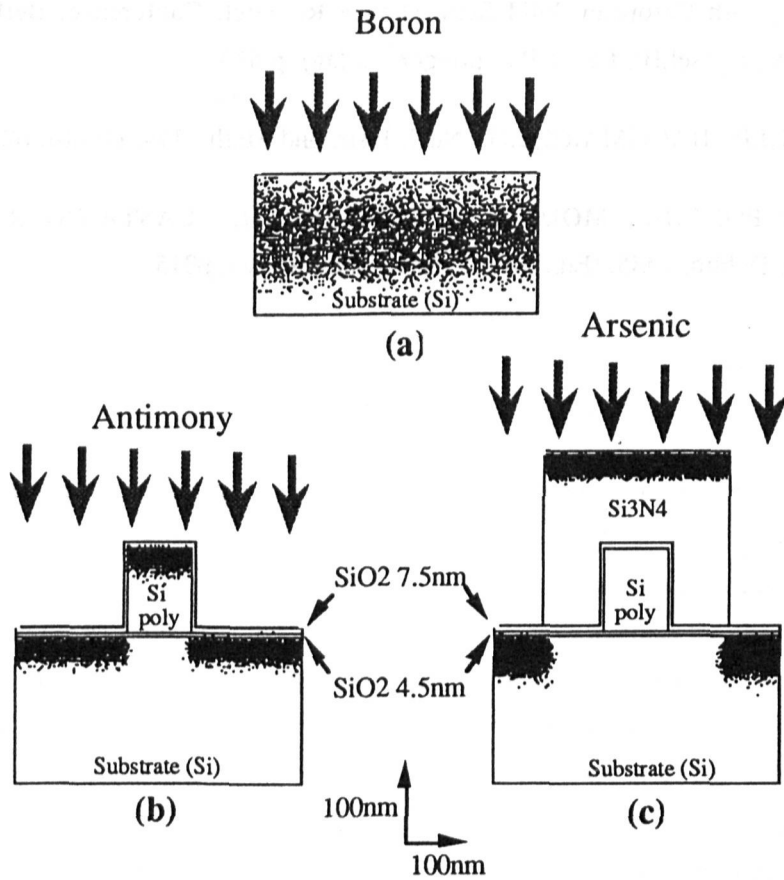


Figure 2: Distribution of the acceptor impurities (Boron: a), and of the donor impurities (Antimony: b and Arsenic: c)

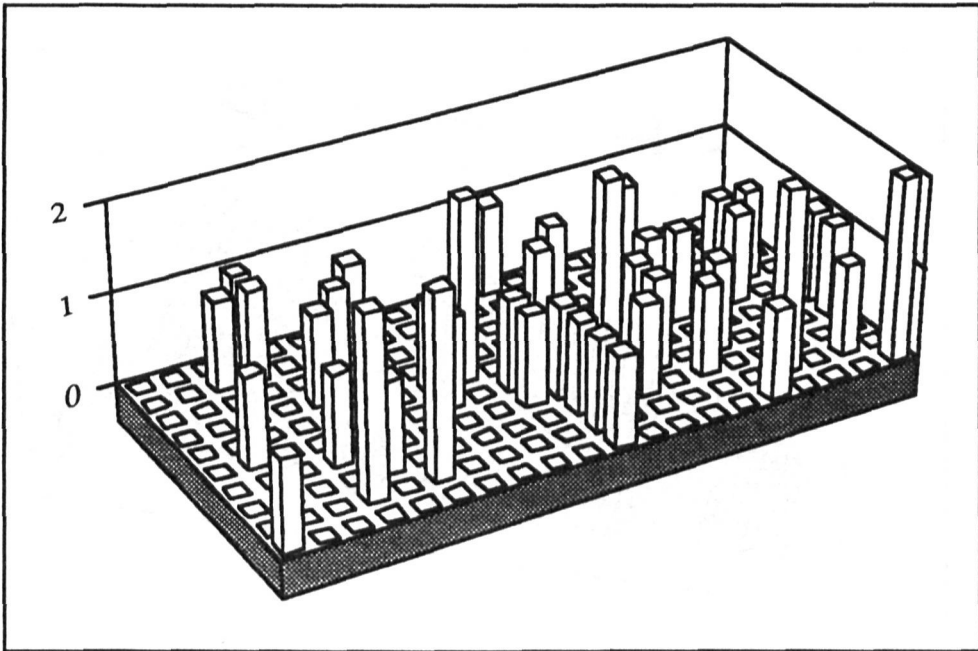


Figure 3: Example of the repartition of the number of boron atoms in the cells of the substrate. The dimensions of a cell are  $2 \times 2.5 \mu\text{m}^2$

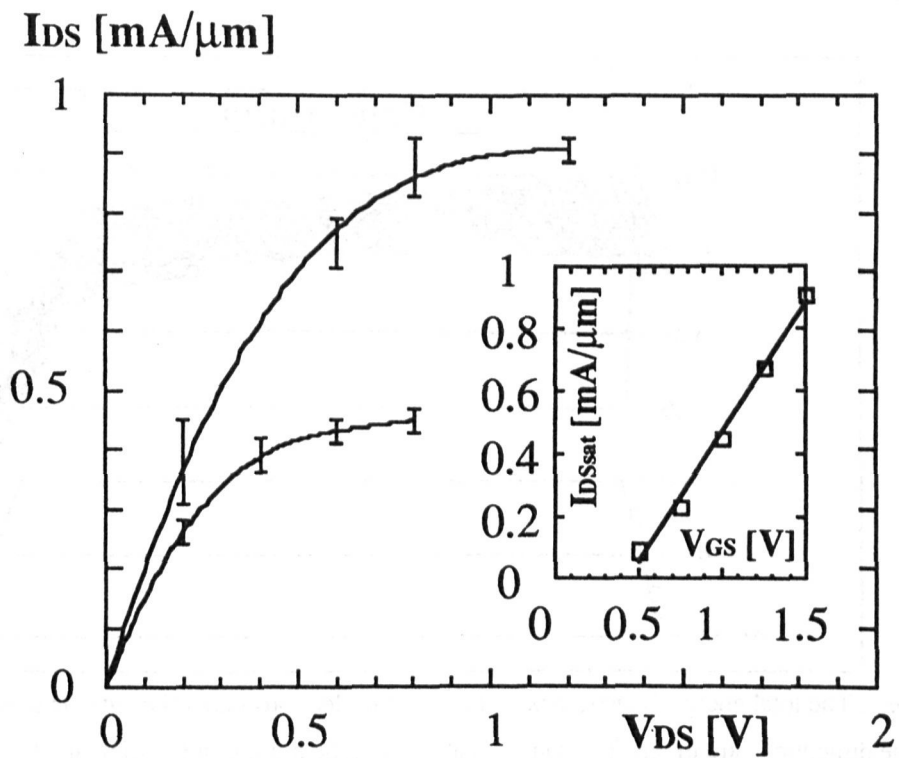


Figure 4: Drain characteristics of the simulated MOSFET for two gate voltages (1V and 1.5V)

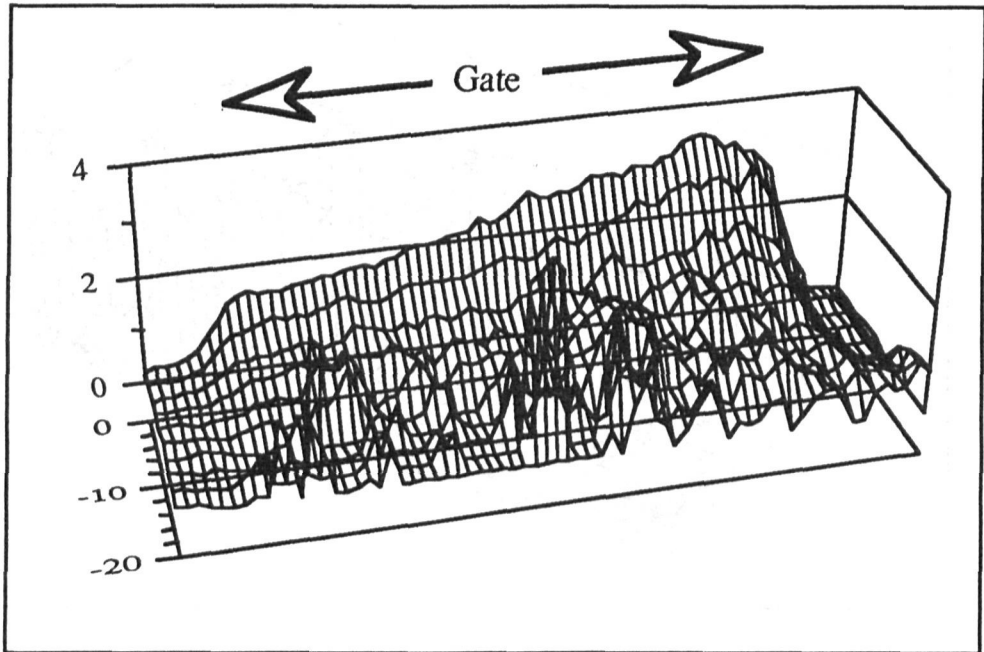


Figure 5: Mean velocity in the source drain direction for the electrons under the gate oxide. The velocities are in  $10^7$  cm/s and the dimensions are in nm. The source is at the left, the drain is at the right and the gate oxide is at the back.

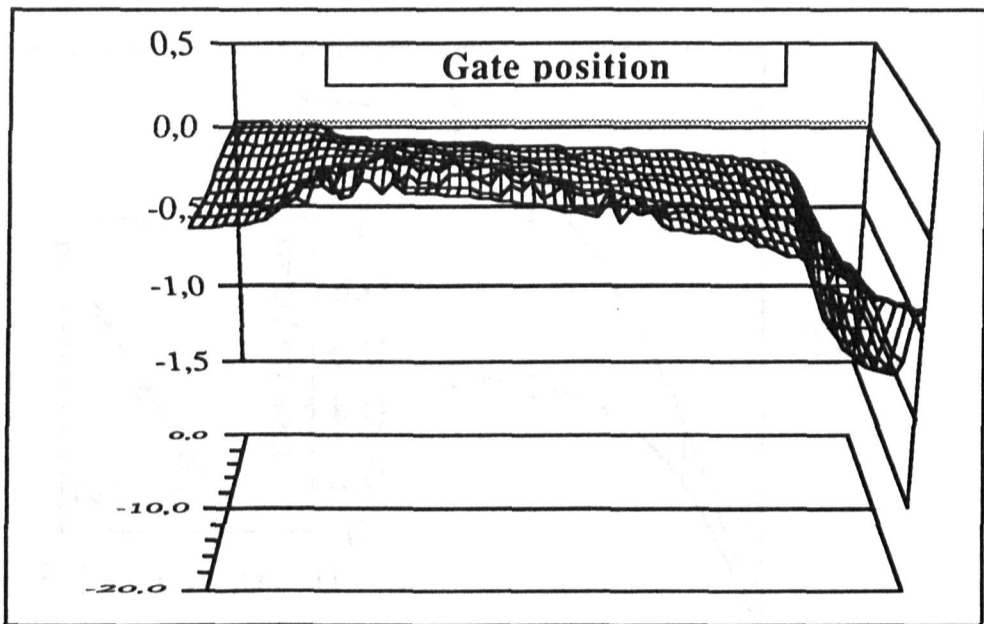


Figure 5: The total energy (kinetic + potential) for the electrons under the gate. The energies are in eV and the dimensions are in nm. The source is at the left, the drain is at the right and the gate oxide is at the back.